LLNL-PROC-676859

LAWRENCE LIVERMORE NATIONAL LABORATORY

Calibration results for first National Ignition Facility Kirkpatrick-Baez Microscope

N. F. Brejnholt, T. Pardini, T. A. Decker, R. M. Hill, L. A. Pickworth, T. J. McCarville, J. J. Ayers, D. K. Bradley, S. P. Hau-Riege, J. K. Vogel, C. C. Walton

September 1, 2015

SPIE Optical Engineering + Applications
San Diego, CA, United States
August 9, 2015 through August 13, 2015

Disclaimer

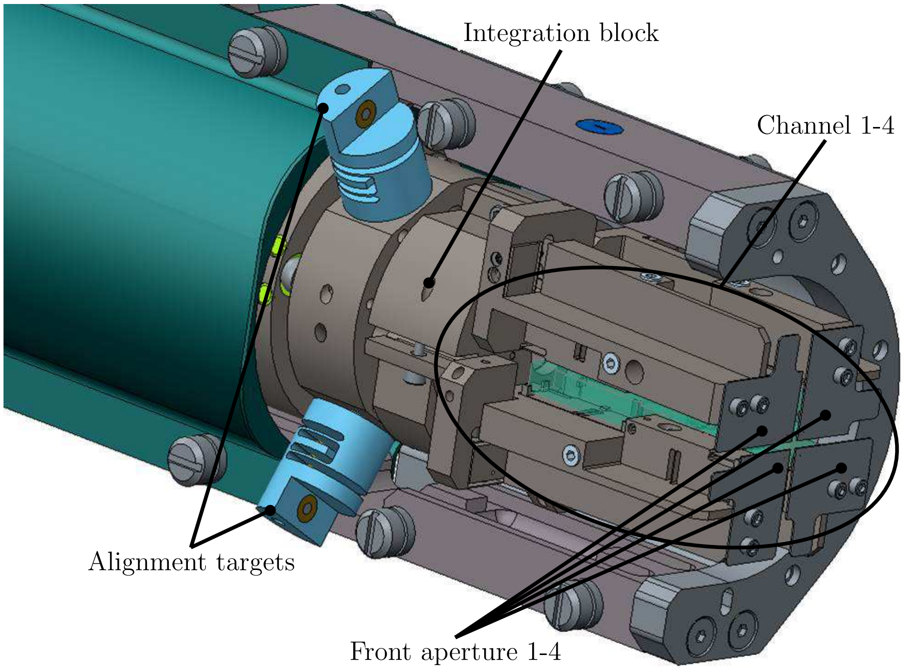

Figure 2: Close-up of the mechnical design of the NIF KBO mirror pack. Four channels, each one containing a KB mirror pair (Figure 1), are mounted in the integration block and pointed to within ±50 μm of the target chamber center at NIF using the alignment targets and the Opposed Port Alignment System (OPAS).[15] Each channel is shown with a 100 μm aperture mounted. For additional details on the mechanical design and alignment at NIF see Ref. 11.

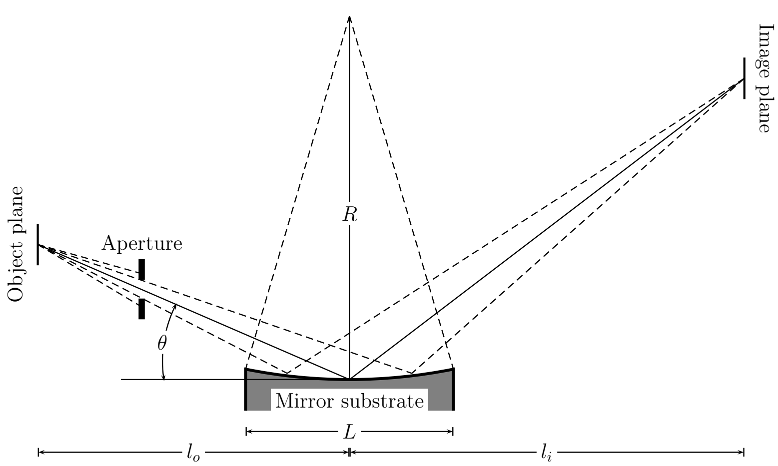

(a)

Parameter	Mirror 1	Mirror 2
l_o	181.0 mm	211.6 mm
l_i	2255.0 mm	2224.4 mm
R	32.0 m	36.9 m
M	12.46×	10.51×

(b)

Figure 3: (a) Simplified illustration of the optical parameters and ray path for a single KB mirror. The mirror length L=30 mm, while the grazing incidence angle $\theta = 0.6°$. The aperture diameter is 100 μm ±0.5 μm which selects an approximately 25 mm long clear aperture. The aperture is crucial for reducing spherical aberrations and consequently improve the spatial resolution. l_o and l_i were optimized to fit within the DIM and provide a magnification on order 12. (b) Optical design parameters for KBO1. The radius of curvature R and magnification M follow from optical principles.

Table 1: Performance goals for KBO1. The spatial resolution is specified at the field of view center (CFOV) and edge (EFOV). The throughput is relative to that achieved with a 10 μm pinhole placed 100 mm from the object plane.

	Goals
Field of view	$\pm 160\ \mu m$
Resolution (CFOV)	$< 5.0\ \mu$m
Resolution (EFOV)	$< 9.0\ \mu$m
Incidence angle θ	$0.6°$
Relative throughput	$10\times$
Center energy	10.3 keV
Spectral bandwidth	± 1.5 keV

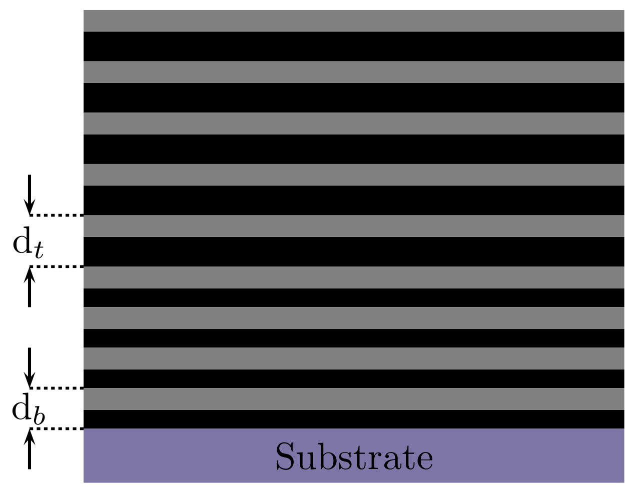

Figure 4: Sketch of the multilayer designed for KBO1 and applied to all substrates. The bottom four bilayer periods are $d_b = 41$ Å$\pm$0.5 Å, while the top five are $d_t = 65$ Å$\pm$1 Å. The heavy material (black) is platinum (Pt) while the spacer layer (gray) is carbon (C).

The second step concerns validation of the assembly and alignment of the individual channels. X-ray imaging tests ensure the mirror pairs are aligned according to the optical design by measuring the spatial resolution over the FOV. The third and final step seeks to find the best drive depth of the KBO1 assembly when being fielded at NIF, i.e. the distance from the object to KBO1, $l_{o,KBO1}$. The optimal drive depth is found as a compromise between the values of l_o (object plane to mirror distance, see Figure 3) for each of the four individual channels. This must be done primarily to mitigate measurement errors in the radius of curvature R of the individual mirrors.

The assembly validation and drive depth sweep were carried out using a custom-built X-ray imaging test bed at LLNL shown in Figure 5. The setup is to scale of the configuration that the KBOs will be fielded in and utilizes a charge-coupled device (CCD) broadly used at NIF.[16] A backlit test grid (Figure 5 inset) with 50 μm pitched features was placed at the nominal object distance l_o. The backlight was Al K-α radiation (1.49 keV) from a Manson X-ray source.[17] KBO1 imaged the grid pattern onto the CCD allowing line outs across the feature edges to be taken. The derived spatial resolution values correspond to the FWHM of this line spread function. For additional details on the calibration setup and methods, refer to Ref. 18.

It is important to note that the CCD pixel pitch is 24 μm. Given the system magnification of $\sim 12\times$, it follows

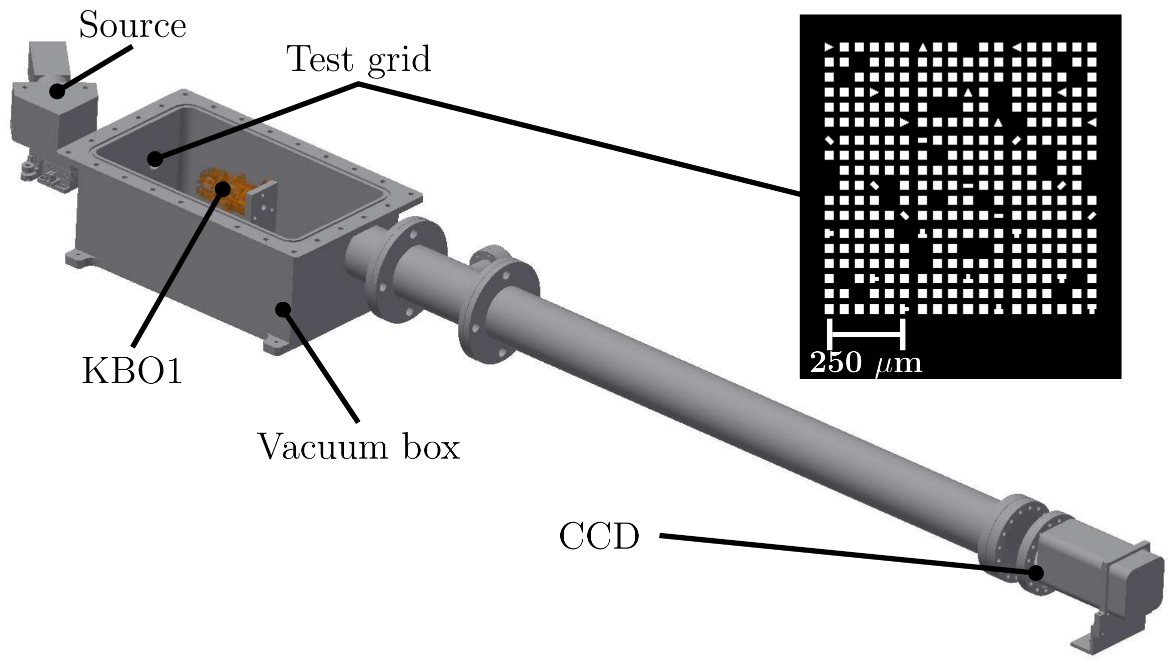

Figure 5: Illustration of the X-ray test bed at LLNL used for calibrating KBO1. The setup is to-scale of the configuration at NIF and has a backlit electroformed nickle test grid installed in place of the object. The source is a Manson X-ray generator operating at 6 kV with an aluminum (Al) target. The inset shows the test grid and is not to scale with the test bed.

that the detector contribution will dominate at the CFOV for a properly aligned KBO, adding approximately 4 μm in quadrature to the minimum achievable resolution. Similarly, diffraction at 1.49 keV contributes on order 2 μm. Resolution values quoted in these proceedings include both of these terms unless otherwise noted.

In the following sections, the approach and results from the calibration campaigns are outlined.

3.1 Multilayer performance

The multilayer performance relies on its adherence to the bilayer period recipe (Figure 4) and the quality of the interfaces. The bilayer recipe is designed to create a flat reflectivity response to 10.3 keV$\pm$1.5 keV photons within the cone of solid angles defined by the aperture using a small number of bilayers. The small number of bilayers acts to reduce the complexity of deposition and decrease the effect of cumulative micro-roughness.[19] Despite the simplicity of the bilayer stack the multilayer may deviate from the design in one of two ways. One is through variation of d_b and d_t (refer to Figure 4) as a function of depth in the stack. Careful calibration of the deposition rate minimize this effect, but systematic offsets of a few percent may still occur. The second design deviation comes through variation, or non-uniformity, in the bilayer period as a function of location on the mirror substrate surface. The small size of the mirror substrate (6.4×30 mm^2) means that this is primarily a concern due to shadowing near the substrate edges.[20]

The uniformity of the coating was characterized by illuminating a number of points (Figure 6a) with a 500×100 μm^2, 800 eV beam at the ALS beamline 6.3.2 reflectometer. The results shown in Figure 6b demonstrated less than $\pm$0.5% non-uniformity within the clear aperture, while an up to 3% reduction in bilayer period was found outside the clear aperture. A systematic offset in bilayer period through the stack of order 1 Å was also observed. Neither of these deviations compromises the multilayer performance but may shift the bandpass slightly towards lower energies.

The quality of the interfaces is another critical multilayer parameter as it governs the reflection efficiency and in turn impacts the KBO throughput. As the 800 eV radiation only probes the top few bilayers and mid-spatial

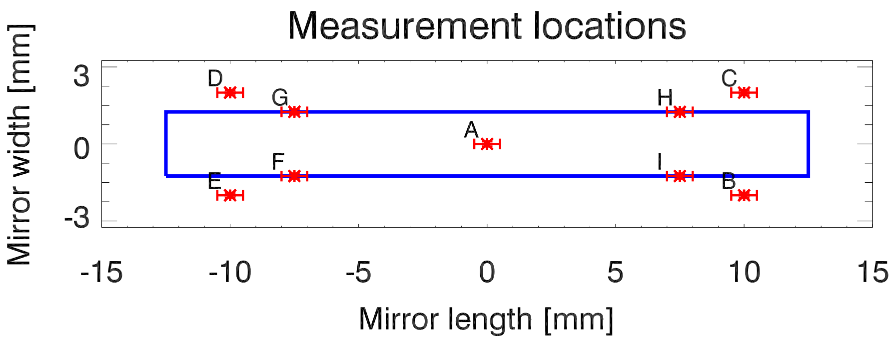

(a)

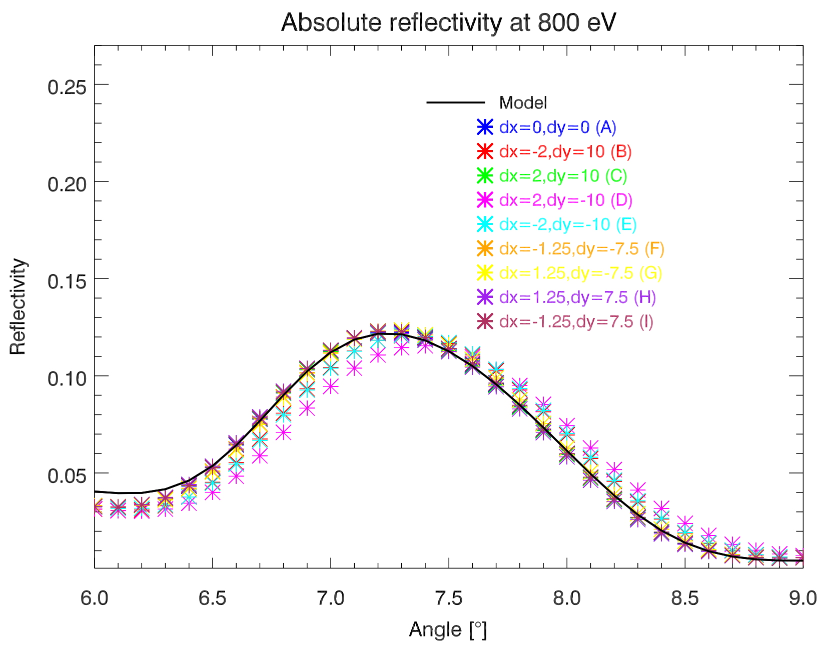

(b)

Figure 6: (a) A to-scale representation of a mirror substrate surface and locations where the absolute reflectivity was determined using 800 eV synchrotron radiation. The clear aperture of the KB is outlined (blue box). Error bars represent synchrotron beam footprint at grazing incidence. (b) Compilation of absolute reflectivity measurements off of a KBO1 coated mirror substrate. Measurements within the clear aperture demonstrate very uniform response.

frequency roughness, Cu K-α radiation was employed to investigate the full stack of bilayers as well as the high-spatial frequency roughness. An example of the results is shown in Figure 7. Overall the multilayers were found to have a typical micro-roughness of 7-7.5 Å rather than the 4.5 Å anticipated from early depositions on super-polished test flats. The main reason for this was a higher-than-specified initial RMS micro-roughness of the bare mirror substrates. The super-polished test flats start out with < 2 Å RMS micro-roughness, whereas the mirror substrates came in at around 3.4 Å. The increase in micro-roughness, and subsequent decrease in multilayer efficiency, led to the KBO1 relative throughput estimate being about half (4.7$\times$ versus 10$\times$) of the intended improvement. Future KBOs, starting with KBO3, will feature mirror substrates with < 2.5 Å RMS micro-roughness which will improve the achievable throughput.

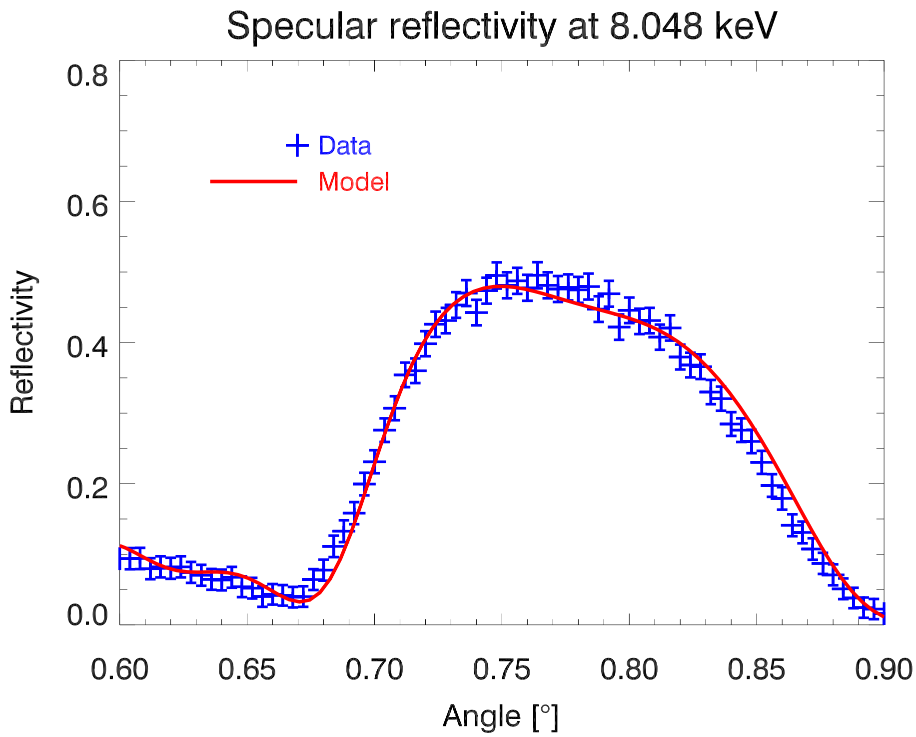

Figure 7: Specular reflectivity acquired on a LLNL-based Cu K-α reflectometer. The model assumes close to the nominal bilayer periods (Figure 4) with a micro-roughness of ~ 7.5 Å. This is significantly higher than the 4.5 Å expected from early depositions on super-polished flats. The increase is caused by a higher-than-specified uncoated substrate RMS micro-roughness and results in the estimated throughput of KBO1 being less than half of the intended.

3.2 Assembly and alignment

Tight alignment tolerances, particularly on the mirror pitch angle, necessitated the use of a coordinate measuring machine (CMM) for the assembly of KBO1. The CMM provides a high accuracy common coordinate system in which the mirrors and their fixtures can be jointly located and positioned to within ± 2 μm of their ideal locations with respect to each other. The apertures (Figure 2) must be placed with similar accuracy (± 5 μm) in the same coordinate system to minimize spherical abberations. For additional details on the assembly and alignment procedures, refer to Ref. 11.

Validation of the CMM alignment can only be done by interrogating the assembled mirror pack with X-rays and estimating the as-built spatial resolution. Figure 8 shows data from a channel prior to corrective actions. The best resolution achieved in this image was ~ 7 μm, i.e. failing to meet the CFOV goal of 5 μm (Table 1) even after subtraction of detector and diffraction contributions. Guided by the X-ray data, inspection with the CMM established that a pitch error on order 170 μrad (equivalent to ~ 5 μm height error) was present. Additional investigations established that further degradation arose from the aperture having shifted by 70 μm from its nominal position. The root cause of both errors was found to be a flexure allowing unintended degrees of freedom. The flexure was fixed in all channels and realignment was carried out resulting in the data shown in Figure 9. Figure 9b demonstrates that the CMM correction led to an improved spatial resolution of approximately 4.9 Å or, subtracting detector and diffraction contributions, ~ 2 Å. The obtained values closely match the predicted best achievable resolution and meets the goal for both CFOV and EFOV. The example data is representative of all channels following realignment.

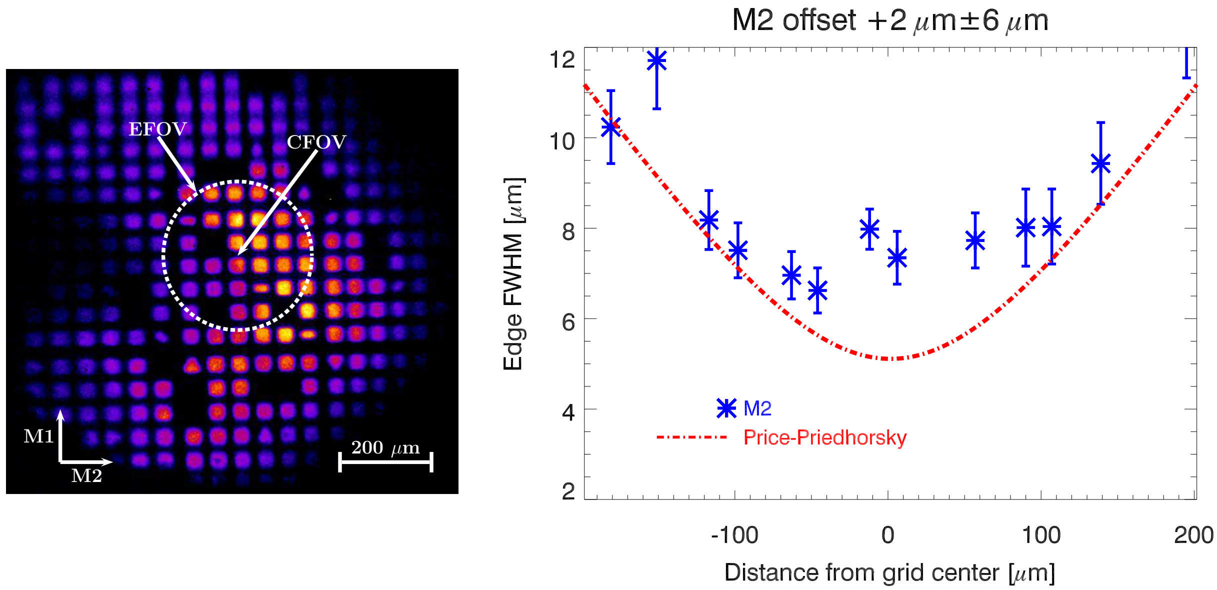

(a) (b)

Figure 8: (a) Composite image created from 35 × 60 s exposures on the X-ray test bed. Mirror 1 (M1) and mirror 2 (M2) direction is indicated along with the location of the center of the field of view (CFOV) and the edge of the field of view (EFOV) as given by Table 1. The data was acquired prior to CMM corrections. The uneven illumination is caused by source non-uniformity. (b) Shows spatial resolution values corresponding to the FWHM of the line spread function across edges along the M2 direction in (a). Results are compared to theoretical values derived using the approach discussed in Ref. 9 and taking into account diffraction and detector terms.

3.3 Drive depth sweep

While the brunt of the pointing of the individual channels follows inherently from the assembly and alignment procedures, the CMM cannot account for errors in mirror optical parameters, specifically R (Figure 3) and in turn the focal length f of the mirrors, as $f = (R sin(\theta))/2$. Consequently, errors in R will propagate to change the optimal drive depth, represented by l_o, of the individual channels in an unknown manner. In a worst case scenario this will lead to only a single channel at a time being pointed to resolve the object.

The objective of the drive depth sweep is to ensure that a compromise between individual channel l_o's is found, i.e. setting $l_{o,KBO1}$ such that all four channels demonstrate good resolution over the same area in the object plane. This mitigation approach must be used as R is fixed and the mirror mounting hardware cannot accommodate changes in individual mirror position along the beam path. With the object size being of order 60 μm, and including a DIM pointing tolerance of ± 50 μm, the CFOVs must be clustered within ± 100 μm of the center of mass (CoM) of the CFOVs to meet the spatial resolution goals (Table 1). Ideally, this value should be below ± 50 μm in order to have good resolution (~ 5 μm) over the full extent of the object in all channels.

Results from the sweep are shown in Figure 10. It was found that the CFOVs were located within ± 80 μm of CoM at the nominal $l_{o,KBO1}$ value of 181 mm. The best compromise was found at $l_{o,KBO1} = 179.4$ mm with the CFOVs being within ± 47 μm of the CoM.

As a sanity check on these values, we consider that with $l_o >> l_i$, the change in focal length Δf, resulting from a radius of curvature measurement error ΔR, is well approximated by the change in l_o. With $\Delta f = (\Delta R \theta)/2$ and $\Delta R \approx 0.5$ m, Δf is approximately ± 2.6 mm for each mirror with respect to design. As such, the 1.6 mm change necessary in l_o is reasonable.

$l_{o,KBO1} = 179.4$ mm implies a lower than specified (Table 1) and measured R. The fact that channel 1-3 all indicate 179.4 mm is close to the optimal value, may imply a systematic error in computing R from interferometric

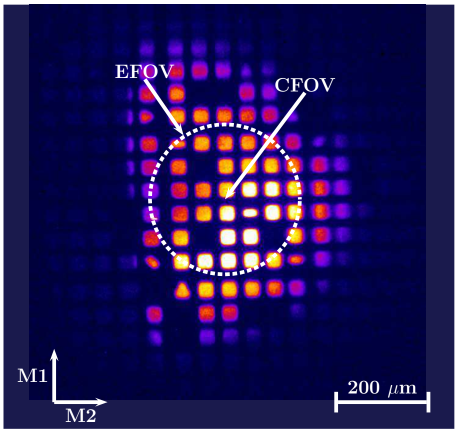

(a)

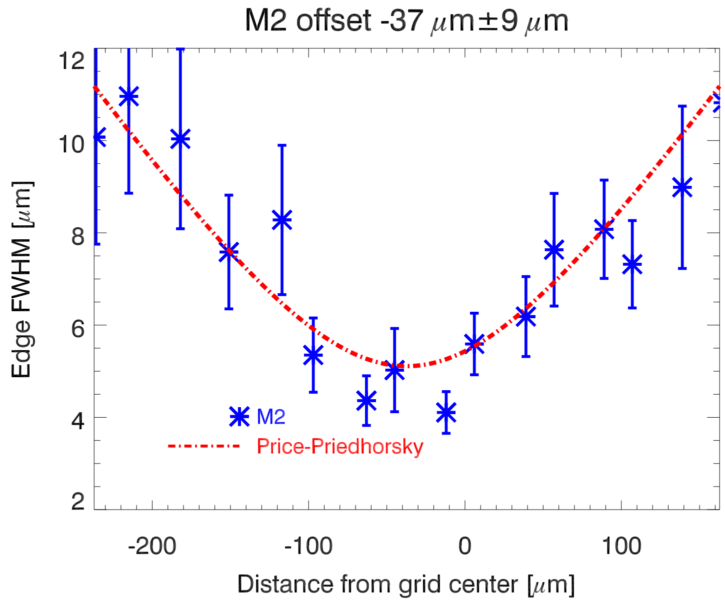

(b)

Figure 9: (a) Composite image created from 100 × 60 s exposures on the X-ray test bed. Mirror 1 (M1) and mirror 2 (M2) direction is indicated along with the location of the center of the field of view (CFOV) and the edge of the field of view (EFOV) as given by Table 1. The data was acquired after several CMM corrections had been implemented guided by previous X-ray results. The uneven illumination is caused by source non-uniformity. (b) Shows spatial resolution values corresponding to the FWHM of the line spread function across edges along the M2 direction in (a). Results are compared to theoretical values derived using the approach discussed in Ref. 9 and taking into account diffraction and detector terms.

data. Improvements to this method are planned for future mirror packs.

4. RESULTS SUMMARY AND CONCLUSIONS

KBO1 has acted as a prototype and demonstrator for a series of KB imagers commissioned by NIF. The performance was investigated prior to fielding at NIF through an extensive off-line calibration campaign described in these proceedings. The main results are summarized in Table 2. The calibration campaign acted to validate and improve the assembly and alignment procedure through determination of the as-built spatial resolution, overcome limitations in determination of optical parameters and to estimate the throughput.

The results show that KBO1 has ~ 2 μm spatial resolution at the center of the field of view and better than 8 μm at the edge (± 160 μm), when subtracting detector and diffraction terms. This exceeds the performance goals (Table 1) for spatial resolution and indicates that achievable spatial resolution at NIF will be limited by detector resolution over much of the field of view. The campaign also estimates that throughput is roughly half of the intended on account of higher-than-specified mirror substrate micro-roughness. Improvements to the substrate surface quality will be in place for KBO3.

The microscope is currently scheduled for alignment shots at NIF in Fall 2015.

Acknowledgment

This work was performed under the auspices of the U.S. Department of Energy by Lawrence Livermore National Laboratory under Contract DE-AC52-07NA27344.

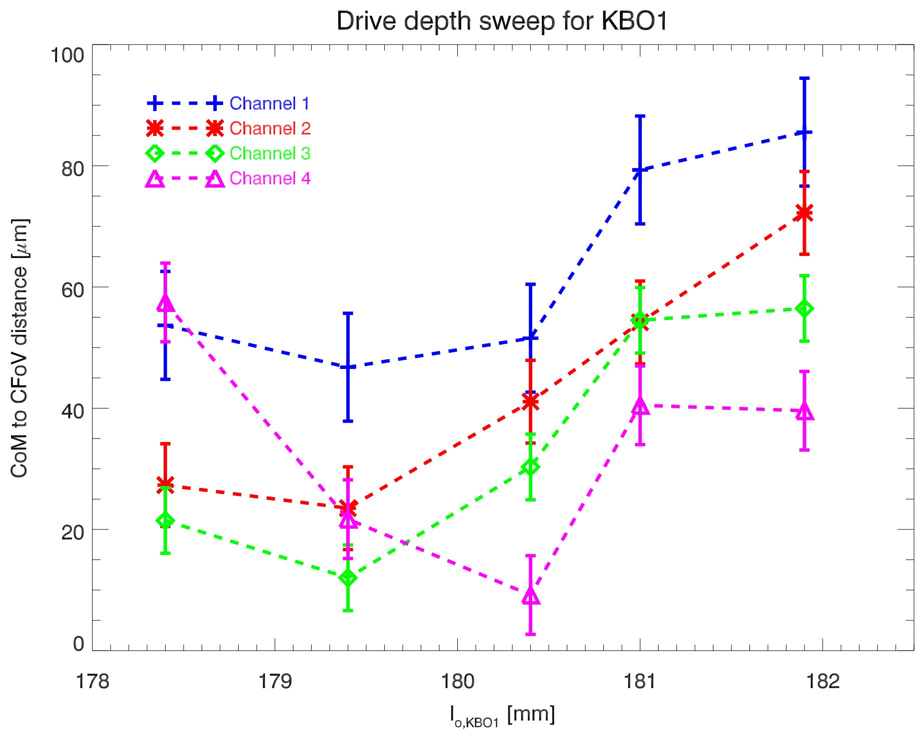

Figure 10: The drive depth $l_{o,KBO1}$ was varied to closely cluster the CFOVs of the individual channels. The clustering is described here through the distance to the COM from individual channel CFOVs and the minimal average value of this was found at l_o=179.4 mm. The data further indicates that all mirrors have lower than measured R, implying a systematic error in determining R.

Table 2: Summary of calibration results. The quoted values are averaged between all four channels. The throughput is relative to a 10 μm pinhole placed 100 mm from the object. Spatial resolution is given in both as-measured values, i.e. including detector and diffraction terms, and in parentheses with these terms subtracted.

	Optic performance
Resolution (CFOV)	4.9 μm (2.0 μm)
Resolution (EFOV)	8.8 μm (7.6 μm)
Center energy	10.3 keV
Spectral bandwidth	$\sim$ 3 keV
Relative throughput	4.7×
$l_{o,KBO1}$	179.4 mm

REFERENCES

1. E. I. Moses, R. N. Boyd, B. A. Remington, C. J. Keane, and R. Al-Ayat, "The national ignition facility: Ushering in a new age for high energy density science," *Phys. Plasmas* **16**(4), p. 041006, 2009.
2. O. L. Landen, J. Edwards, S. W. Haan, H. F. Robey, J. Milovich, B. K. Spears, S. V. Weber, D. S. Clark, J. D. Lindl, B. J. MacGowan, and et al., "Capsule implosion optimization during the indirect-drive national ignition campaign," *Phys. Plasmas* **18**(5), p. 051002, 2011.
3. J. R. Rygg, O. S. Jones, J. E. Field, M. A. Barrios, L. R. Benedetti, G. W. Collins, D. C. Eder, M. J. Edwards, J. L. Kline, J. J. Kroll, and et al., "2D X-Ray Radiography of Imploding Capsules at the National Ignition Facility," *Physical Review Letters* **112**, May 2014.

4. T. Ma, N. Izumi, R. Tommasini, D. K. Bradley, P. Bell, C. J. Cerjan, S. Dixit, T. Doppner, O. Jones, J. L. Kline, and et al., "Imaging of high-energy x-ray emission from cryogenic thermonuclear fuel implosions on the NIF," *Review of Scientific Instruments* **83**(10), p. 10E115, 2012.
5. F. J. Marshall and Q. Su, "Quantitative measurements with X-ray microscopes in laser-fusion experiments," *Review of Scientific Instruments* **66**(1), p. 725, 1995.
6. F. J. Marshall and G. R. Bennett, "A high-energy X-ray microscope for inertial confinement fusion," *Review of Scientific Instruments* **70**(1), p. 617, 1999.
7. O. V. Gotchev, L. J. Hayes, P. A. Jaanimagi, J. P. Knauer, F. J. Marshall, and D. D. Meyerhofer, "Large-grazing-angle, multi-image Kirkpatrick-Baez microscope as the front end to a high-resolution streak camera for OMEGA," *Review of Scientific Instruments* **74**(12), p. 5065, 2003.
8. P. Kirkpatrick and A. V. Baez, "Formation of Optical Images by X-Rays," *J. Opt. Soc. Am.* **38**, p. 766, Sep 1948.
9. R. Price and W. Priedhorsky, "Kirkpatrick-Baez X-ray microscope optimization for inertial-confinement-fusion applications," Tech. Rep. UCID-19831, Lawrence Livermore National Laboratory, 1983.
10. V. A. Smalyuk, S. V. Weber, D. T. Casey, D. S. Clark, J. E. Field, S. W. Haan, B. A. Hammel, A. V. Hamza, D. E. Hoover, O. L. Landen, and et al., "Hydrodynamic instability growth of three-dimensional, native-roughness modulations in x-ray driven, spherical implosions at the National Ignition Facility," *Phys. Plasmas* **22**, p. 072704, Jul 2015.
11. M. J. Ayers, L. A. Pickworth, T. Decker, R. Hill, T. Pardini, T. McCarville, N. Shingleton, C. Smith, C. G. Bailey, P. M. Bell, and et al., "Engineering precision relocation capability into a large-cantilevered telescoping diagnostic for a Kirkpatrick Baez X-ray Optic," *Target Diagnostics Physics and Engineering for Inertial Confinement Fusion III* , Sep 2014.
12. D. G. Stearns, "The scattering of X-rays from nonideal multilayer structures," *Journal of Applied Physics* **65**(2), p. 491, 1989.
13. D. L. Windt, "IMD - Software for modeling the optical properties of multilayer films," *Comput. Phys.* **12**, p. 360, 1998.
14. T. Pardini, T. J. McCarville, C. C. Walton, T. A. Decker, J. K. Vogel, P. B. Mirkarimi, J. B. Alameda, R. M. Hill, L. A. Pickworth, V. A. Smalyuk, and et al., "Optical and multilayer design for the first Kirkpatrick-Baez optics for X-ray diagnostic at NIF," *Target Diagnostics Physics and Engineering for Inertial Confinement Fusion II* , Sep 2013.
15. A. M. Manuel, T. J. McCarville, L. G. Seppala, J. L. Klingmann, and D. H. Kalantar, "Opposed port alignment system (OPAS): a commercial astronomical telescope modified for viewing the interior of the NIF target chamber," *Optical System Alignment, Tolerancing, and Verification VI* , Oct 2012.
16. M. D. Landon, J. A. Koch, S. S. Alvarez, P. M. Bell, F. D. Lee, and J. D. Moody, "Design of the National Ignition Facility static X-ray imager," *Review of Scientific Instruments* **72**(1), p. 698, 2001.
17. M. J. Haugh and M. B. Schneider, "Flat field anomalies in an X-ray charge coupled device camera measured using a Manson X-ray source," *Review of Scientific Instruments* **79**(10), p. 10E925, 2008.
18. L. A. Pickworth, T. McCarville, T. Decker, T. Pardini, J. Ayers, P. Bell, D. Bradley, N. F. Brejnholt, N. Izumi, P. Mirkarimi, and et al., "A kirkpatrick-baez microscope for the national ignition facilitya)," *Review of Scientific Instruments* **85**, p. 11D611, Nov 2014.
19. D. G. Stearns, D. P. Gaines, D. W. Sweeney, and E. M. Gullikson, "Nonspecular x-ray scattering in a multilayer-coated imaging system," *Journal of Applied Physics* **84**(2), p. 1003, 1998.
20. D. Martinez-Galarce, R. Soufli, D. L. Windt, M. Bruner, E. Gullikson, S. Khatri, E. Spiller, J. C. Robinson, S. Baker, and E. Prast, "Multisegmented, multilayer-coated mirrors for the solar ultraviolet imager," *Opt. Eng* **52**, p. 095102, Sep 2013.